Magnetopiezotransmission Studies of the Indirect Transition in Germanium

R. L. AGGARWAL, M. D. ZUTECK,* AND BENJAMIN LAX†
Francis Bitter National Magnet Laboratory,‡ Massachusetts Institute of Technology, Cambridge, Massachusetts 02139
(Received 11 June 1968)

The indirect transition in germanium at $T\sim20°K$ has been examined with magnetic fields up to 90 kG, using the high-sensitivity piezotransmission technique. Samples were in the Voigt configuration in which the Poynting vector of the radiation field is perpendicular to the applied magnetic field. The spectra recorded with light polarized either parallel or perpendicular to the magnetic field applied along a [001], [111], or [110] direction exhibit a series of sharp peaks, in contrast to the corresponding series of less distinct steps which are observed in the conventional magnetoabsorption spectra for the indirect edge. At high magnetic fields the piezotransmission peaks have been resolved over a spectral range of more than 0.1 eV which extends from the zero-field edge at 0.77 eV to photon energies at which the direct transition dominates. From the energy spacings of the peaks, we have deduced the cyclotron effective mass m_c for the L_1 conduction band and its variation as a function of the energy $\mathcal{E}$ measured from the bottom of the band. For large $\mathcal{E}$, m_c is found to vary linearly with $\mathcal{E}$, in agreement with the results of the $\langle k\cdot p\rangle$ perturbation analysis. But the observed slope of the m_c-versus-$\mathcal{E}$ curve is greater than that expected from theory. Linear extrapolation of the experimental curve gives for the effective mass at the bottom of the band $m_c(0)=(0.129\pm0.002)m_0$ for $\mathbf{H}\|[001]$. Similarly, for $\mathbf{H}\|[111]$ and [110], we obtain for the light electron mass at the bottom of the conduction band $m_{le}(0)=(0.079\pm0.001)m_0$ and $(0.095\pm0.001)m_0$, respectively. Assuming that the ratio of the longitudinal to the transverse effective masses is $m_l(0)/m_t(0)\simeq20$, the above values for $m_c(0)$ and $m_{le}(0)$ give the transverse effective mass $m_t(0)=(0.078\pm0.002)m_0$, $(0.079\pm0.001)m_0$, and $(0.079\pm0.001)m_0$ for $\mathbf{H}\|[001]$, [111], and [110], respectively. m_l has been estimated from the series of peaks due to the heavy electron mass. Using an average value for $m_{he}/m_0=0.352$ with $\mathbf{H}\|[110]$, we find that $m_l/m_0=1.54\pm0.06$.

I. INTRODUCTION

THE indirect edge due to the phonon-assisted optical transitions between the valence band at the Γ point and the L_1 conduction band in germanium has been the subject of several investigations.[1–8] The effect of an applied magnetic field on the indirect transition was first observed by Zwerdling *et al.*[4] with fields up to 39 kG and later by Halpern[5,6] with magnetic fields as high as 74 kG. The magnetoabsorption spectra exhibit one or more series of oscillations due to transitions from the quantized Landau levels near the top of the valence band to those of the conduction band. The observed energy spacings between the peaks of the magnetoabsorption spectra were used for a determination of the electron effective masses.[6] Since magneto-oscillations, even under the most favorable conditions of low temperatures and high magnetic fields, were observed only at photon energies close to the edge,[6] it was not possible to study the effective masses at energies other than those corresponding to the band extrema. This limitation may be overcome by employing one of the several modulation techniques[8–15] that have been used very successfully in the observation of interband magneto-optical transitions at photon energies far removed from the band edge.[9,16–21]

We have used the stress modulation technique[8,12] to examine the indirect transition in germanium at low temperatures with magnetic fields up to 90 kG. Magnetopiezotransmission spectra exhibit sharp oscillations up to photon energies at which the direct transition dominates. The observation of magneto-oscillations at

* Present address: Department of Physics, University of Illinois, Urbana, Ill.
† Also Physics Department, Massachusetts Institute of Technology, Cambridge, Mass.
‡ Supported by the U. S. Air Force Office of Scientific Research.
[1] G. G. Macfarlane, T. P. McLean, J. E. Quarrington, and V. Roberts, Phys. Rev. **108**, 1377 (1957); Proc. Phys. Soc. (London) **71**, 863 (1958); J. Phys. Chem. Solids **8**, 388 (1959).
[2] L. H. Hall, J. Bardeen, and F. J. Blatt, Phys. Rev. **95**, 559 (1954); in *Proceedings of the Conference on Photoconductivity, Atlantic City, 1954*, edited by R. G. Breckenridge, B. R. Russell, and E. E. Hahn (John Wiley & Sons, Inc., New York, 1956), p. 146.
[3] R. J. Elliot, T. P. McLean, and G. G. Macfarlane, Proc. Phys. Soc. (London) **72**, 553 (1958).
[4] S. Zwerdling, B. Lax, L. M. Roth, and K. J. Button, Phys. Rev. **114**, 80 (1959).
[5] J. Halpern, Ph.D. thesis, Massachusetts Institute of Technology, 1964 (unpublished).
[6] J. Halpern and B. Lax, J. Phys. Chem. Solids **26**, 911 (1965).
[7] I. Balslev, Phys. Rev. **143**, 636 (1966).
[8] W. E. Engeler, M. Garfinkel, and J. J. Tiemann, Phys. Rev. Letters **16**, 239 (1966); Phys. Rev. **155**, 693 (1967).
[9] Q. H. F. Vrehen, and B. Lax, Phys. Rev. Letters **12**, 471 (1964).
[10] A. Frova and P. Handler, in *Proceedings of the Internal Conference on the Physics of Semiconductors, Paris, 1964* (Academic Press Inc., New York, 1965), p. 157.
[11] B. O. Seraphin and R. B. Hess, Phys. Rev. Letters **14**, 138 (1965); B. O. Seraphin and N. Bottka, *ibid.* **15**, 104 (1965).
[12] W. E. Engeler, H. Fritzsche, M. Garfinkel, and J. J. Tiemann, Phys. Rev. Letters **14**, 1069 (1965).
[13] G. W. Gobeli and E. O. Kane, Phys. Rev. Letters **15**, 142 (1965).
[14] K. L. Shaklee, F. H. Pollak, and M. Cardona, Phys. Rev. Letters **15**, 883 (1965).
[15] B. Batz, Solid State Commun. **4**, 241 (1966).
[16] R. L. Aggarwal, L. Rubin, and B. Lax, Phys. Rev. Letters **17**, 8 (1966).
[17] J. G. Mavroides, M. S. Dresselhaus, R. L. Aggarwal, and G. F. Dresselhaus, J. Phys. Soc. Japan Suppl. **21**, 184 (1966).
[18] S. H. Groves, C. R. Pidgeon, and J. Feinleib, Phys. Rev. Letters **17**, 643 (1966).
[19] R. L. Aggarwal and B. Lax, Bull. Am. Phys. Soc. **11**, 828 (1966).
[20] R. L. Aggarwal, Bull. Am. Phys. Soc. **12**, 100 (1967).
[21] C. R. Pidgeon, S. H. Groves, and J. Feinleib, Solid State Commun. **5**, 677 (1967).

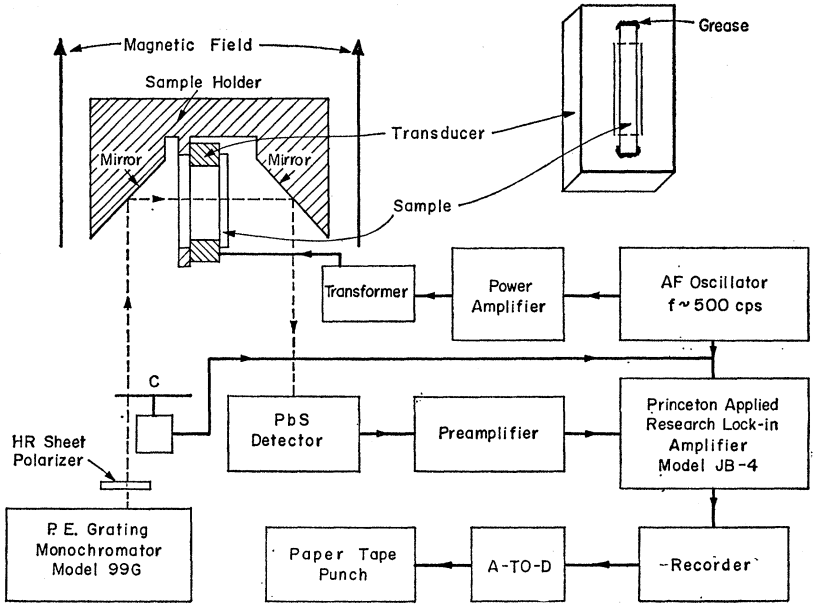

FIG. 1. Schematic diagram of the experimental setup for magnetopiezotransmission experiments. A-to-D: analog-to-digital converter; C: chopper for conventional operation at 150 cps instead of the 13-cps chopper in the monochromator.

energies higher than those investigated before[6] has made possible a determination of the electron effective mass as a function of the energy relative to the band edge. Preliminary results for the nonparabolicity of the L_1 conduction band have been reported previously.[22] The purpose of the present paper is to give a more detailed account of this work. The experimental results are presented in Sec. IV, following a theoretical review in Sec. III of the energy bands in germanium subjected to applied magnetic field and uniaxial stress.

II. EXPERIMENTAL PROCEDURE

A schematic diagram of the experimental apparatus used for the magnetopiezotransmission experiments is given in Fig. 1. The present setup is very similar to that used for magnetopiezoreflection previously.[16] Light from a ribbon-type tungsten filament is focused on the entrance slit of a Perkin-Elmer monochromator equipped with a Bausch and Lomb grating blazed for 1.6 μ. Unchopped double-pass radiation from the monochromator is focused by a suitable combination of plane and spherical mirrors on the specimen which is positioned at the center of a 4-in. Bitter solenoid for magnetic fields up to 90 kG. A Polaroid HR sheet polarizer[23] is used to orient the electric vector of the infrared (IR) radiation either parallel or perpendicular to the applied stress and the magnetic field.

The mechanical stress is applied to the sample by means of a lead-zirconate-titanate-type piezoelectric transducer. The sample is attached to one face of the transducer by means of vacuum grease applied to its two ends (see Fig. 1) for the application of uniaxial stress to the sample. The grease is used to ensure a rigid bond at the low temperatures and to minimize the static stress introduced due to the differential contraction between the sample and the transducer during the cooling process. The transducer is held in direct contact with the flat surface of a copper mounting block in order to achieve good thermal conduction. A hole is cut in both the transducer and the mounting block so that the radiation may be transmitted through the sample. The entire mounting block including the sample, the transducer, and a pair of diagonal mirrors is mounted on the cold finger of an optical cryostat. With liquid helium as the coolant, the sample temperature was estimated to be $\sim$20°K. A periodic uniaxial stress is impressed upon the sample by driving the transducer sinusoidally with an audio oscillator. A peak-to-peak strain of $\sim 7\times10^{-5}$ at 500 cps was used in the present experiments.

The radiation transmitted through the sample is focused on a PbS detector operating at room tempea-e ture. The detector output is amplified by a low-noirs broad-band amplifier. The signal is then fed into a phase-sensitive amplifier PAR model JB-4.[24] The reference signal for the JB-4 is obtained from the oscillator driving the transducer. The output of the JB-4 drives a recorder which in turn feeds a digital data recording system. Each set of data was obtained by sweeping the photon energy of the radiation over the desired spectral range at a constant magnetic field. The recorder signal is proportional to the change in transmission ΔT. In order to obtain the physically interesting quantity $\Delta T/T$, a second scan is made over the same energy range

[22] R. L. Aggarwal, M. D. Zuteck, and B. Lax, Phys. Rev. Letters 19, 236 (1967).

[23] Polaroid Corp., Cambridge, Mass. 02139.

[24] Princeton Applied Research Corporation, Princeton, N. J. 08540.

TABLE I. Electron effective masses and conduction-band-edge splittings in uniaxially stressed germanium.

Direction of stress and magnetic field	Valley(s)	ΔE_c	m_{le}	m_c	m_{he}
[001]	Any	$(\Xi_d+\frac{1}{3}\Xi_u)(e_{xx}+e_{yy}+e_{zz})$		$\sqrt{3}m_t(1+2m_t/m_l)^{-1/2}$	
[111]	1	$(\Xi_d+\frac{1}{3}\Xi_u)(e_{xx}+e_{yy}+e_{zz})$ $+\frac{2}{3}\Xi_u(e_{xy}+e_{yz}+e_{zx})$	m_t		...
	2,3,4	$(\Xi_d+\frac{1}{3}\Xi_u)(e_{xx}+e_{yy}+e_{zz})$ $-2/9\Xi_u(e_{xy}+e_{yz}+e_{zx})$	...		$3m_t(1+8m_t/m_l)^{-1/2}$
[110]	1,3	$(\Xi_d+\frac{1}{3}\Xi_u)(e_{xx}+e_{yy}+e_{zz})+\frac{2}{3}\Xi_u e_{xy}$	$(\sqrt{\frac{8}{9}})m_t(1+m_t/2m_l)^{-1/2}$		...
	2,4	$(\Xi_d+\frac{1}{3}\Xi_u)(e_{xx}+e_{yy}+e_{zz})-\frac{2}{3}\Xi_u e_{xy}$	...		$(m_t m_l)^{1/2}$

without any stress modulation applied to the sample. The light incident on the sample was in this case chopped at a frequency of $\sim$150 cps and the phase-sensitive amplifier was tuned for the 150-cps signal. The digitized output for the above two scans was then processed with the help of an IBM 7094 computer to obtain $\Delta T/T$, which was subsequently plotted as a function of the photon energy by the Calcomp incremental plotter.

Single-crystal specimens of high-purity germanium ($\rho\simeq$40 Ω cm at 300°K) were used in the experiments. The samples were x-ray-oriented, and were sliced and lapped so that their dimensions were approximately 20 mm in length, 3 mm in width, and 0.4 mm in thickness. During the lapping process, the sample thickness was ground to a $\frac{1}{2}°$ wedge in order to avoid interference effects in the transmitted light due to multiple reflections from the front and back surfaces of the sample. After lapping, the samples were etched for $\sim$1–2 min. in a solution of HNO_3 and HF mixed in the ratio of 3:1.

III. THEORETICAL CONSIDERATIONS

The indirect absorption edge in germanium is due to transitions between the valence-band states at the center of the Brillouin zone and the conduction-band minima at the L points which lie along the ⟨111⟩ crystallographic directions at the zone edge.[25] Such transitions occur via an intermediate state with the emission or absorption of a phonon in order to conserve total momentum in the initial and final states.[1,2] Before considering the increase in sensitivity obtained by the use of the piezotransmission technique for the observation of indirect transitions with and without magnetic field, we will briefly present the results of uniaxial stress and magnetic field on the conduction- and valence-band edges which are required for the analysis of the experimental data.

A. Energy Levels in Uniaxially Stressed Germanium Subjected to External Magnetic Field

1. L_1 Conduction Band

In the absence of uniaxial stress and magnetic field, the surfaces of constant energy in the vicinity of the conduction-band minima in k space are ellipsoids of the form

$$\mathcal{E}(\mathbf{k})=\frac{\hbar^2}{2m_t}(k_1^2+k_2^2)+\frac{\hbar^2}{2m_l}k_3^2, \quad (1)$$

where 1, 2, and 3 define three mutually perpendicular axes such that axis 3 is along the longitudinal direction of the ellipsoidal energy surface; m_l and m_t are the electron effective masses parallel and perpendicular to the longitudinal axis; and k_1, k_2, and k_3 are the components of the electron wave vector $\mathbf{k}$ relative to that for the center of the ellipsoidal surface.

As in the case of free carriers, the application of a homogeneous magnetic field produces a series of quantized one-dimensional sub-bands for electrons with the ellipsoidal energy surfaces of Eq. (1). Using the effective-mass approximation of Luttinger and Kohn,[26] the energy levels for the ith ellipsoid are given by[3,27]

$$\mathcal{E}_n^{(i)}(k)=(n+\tfrac{1}{2})\hbar\omega_c^{(i)}+\hbar^2k_z^2/2m_z^{(i)}\pm\tfrac{1}{2}\beta g_z^{(i)}H, \quad (2)$$

with $\omega_c^{(i)}=eH/m_c^{(i)}c$, where the superscript (i) denotes the ellipsoid under consideration; ω_c and m_c are the cyclotron frequency and the cyclotron effective mass, respectively; $n=0$, 1, 2, etc., denotes the Landau quantum number, and k_z and m_z are the electron momentum and effective mass in the direction of the magnetic field, respectively; $\beta=e\hbar/2m_0c$, where m_0 is the free-electron mass; and g_z is the spectroscopic splitting factor parallel to the magnetic field. $m_c^{(i)}$ and $m_z^{(i)}$ are given in terms of m_t and m_l as

$$m_c^{(i)}=m_t[m_l/(m_l\cos^2\theta^{(i)}+m_t\sin^2\theta^{(i)})]^{1/2}, \quad (3a)$$

$$m_z^{(i)}=m_l\cos^2\theta^{(i)}+m_t\sin^2\theta^{(i)}, \quad (3b)$$

where $\theta^{(i)}$ represents the angle between the applied magnetic field and the longitudinal axis of the ith ellipsoid. Thus the cyclotron effective masses are not equal for all the ellipsoids except when the magnetic field is along a cubic axis, in which case

$$m_c=\sqrt{3}m_t(1+2m_t/m_l)^{-1/2}. \quad (4)$$

[25] B. Lax, H. J. Zeiger, R. N. Dexter, and E. S. Rosenblum, Phys. Rev. 93, 1418 (1954).

[26] J. M. Luttinger and W. Kohn, Phys. Rev. 97, 869 (1955).

[27] B. Lax, in *Proceedings of the "Enrico Fermi" International School of Physics, Course XXII*, edited by R. A. Smith (Academic Press Inc., New York, 1963), p. 240.

For the magnetic field along a [111] or [110] direction, the four ellipsoids are divided into two groups with distinct cyclotron frequencies corresponding to a light electron mass m_{le} and a heavy electron mass m_{he}. If the four valleys with their major axes along [111], [1$\bar{1}\bar{1}$], [$\bar{1}$1$\bar{1}$], and [$\bar{1}\bar{1}$1] are labelled as 1, 2, 3, and 4, respectively, it can be easily shown from Eq. (3a) that for $m_l > m_t$ we obtain for $\mathbf{H}\|[111]$

$$\begin{aligned} m_{le} &= m_c^{(1)}, \\ m_{he} &= m_c^{(2)} = m_c^{(3)} = m_c^{(4)}. \end{aligned} \tag{5a}$$

Similarly, for $\mathbf{H}\|[110]$,

$$\begin{aligned} m_{le} &= m_c^{(1)} = m_c^{(3)}, \\ m_{he} &= m_c^{(2)} = m_c^{(4)}. \end{aligned} \tag{5b}$$

These masses as deduced from Eq. (3a), using $m_l/m_t \simeq 20$,[28] are summarized in Table I.

In the absence of external magnetic field the application of uniaxial stress along an arbitrary direction in the crystal would destroy the energy equivalence of the ⟨111⟩ ellipsoids. Following Herring's deformation-potential analysis,[29,30] one can write the shift in energy of the ith minimum as[31]

$$\Delta\epsilon_c^{(i)} = \sum_{\alpha\beta} [\Xi_d \delta_{\alpha\beta} + \Xi_u K_\alpha^{(i)} K_\beta^{(i)}] e_{\alpha\beta}, \tag{6}$$

where Ξ_d is the deformation potential for dilation and Ξ_u for shear, $K_\alpha^{(i)}$ are the components of a unit vector pointing from the center of the Brillouin zone toward the position in k space of the ith minimum, and $e_{\alpha\beta}$ are the components of the strain tensor.[32] The subindices α and β refer to the cubic axes of the crystal.

We will now consider the special cases where the stress T is applied along the principal crystallographic directions. For $T\|[001]$ the strain components are[31]

$$\begin{aligned} e_{xx} &= e_{yy} = S_{12} T, \\ e_{zz} &= S_{11} T, \\ e_{xy} &= e_{yz} = e_{zx} = 0, \end{aligned} \tag{7}$$

where S_{11} and S_{12} are the compliance constants. Using the strain components given above, it follows from Eq. (6) that stress applied along a cubic axis does not lift the degeneracy of the conduction-band minima but merely shifts the edge by

$$\Delta\epsilon_c = (\Xi_d + \tfrac{1}{3}\Xi_u)(e_{xx} + e_{yy} + e_{zz}). \tag{8}$$

For $T\|[111]$, the strain components are[31]

$$\begin{aligned} e_{xx} &= e_{yy} = e_{zz} = \tfrac{1}{3}(S_{11} + 2S_{12}) T, \\ e_{xy} &= e_{yz} = e_{zx} = \tfrac{1}{6} S_{44} T, \end{aligned} \tag{9}$$

and for $T\|[110]$

$$\begin{aligned} e_{xx} &= e_{yy} = \tfrac{1}{2}(S_{11} + S_{12}) T, \\ e_{zz} &= S_{12} T, \\ e_{xy} &= \tfrac{1}{4} S_{44} T, \quad e_{yz} = e_{zx} = 0. \end{aligned} \tag{10}$$

Using Eqs. (9) and (10), it is shown from Eq. (6) that a [111] or [110] uniaxial stress causes a splitting of the band edge in addition to a shift in the mean energy of the band minima. Total stress-induced energy changes for all the valleys are given in Table I.

From the results summarized in Table I it is obvious that the uniaxial stress applied parallel to the magnetic field does not affect the degeneracies of the Landau-level series for the conduction band. It simply raises or lowers the different Landau ladders with respect to one another.

2. *Valence Band near $k=0$*

In the absence of strain and spin-orbit interaction the top of the valence band occurs at the center of the Brillouin zone and is threefold-degenerate, corresponding to p bonding orbitals on the germanium atoms.[33] The sixfold-degenerate state (including twofold spin degeneracy) is split by spin-orbit interaction into a fourfold $p_{3/2}$ state (Γ_8^+) and a twofold $p_{1/2}$ state (Γ_7^+) lying below it.[34,35] Using the ⟨$\mathbf{k}\cdot\mathbf{p}$⟩ perturbation theory, Dresselhaus, Kip, and Kittel obtained, near $k=0$, energy surfaces of the form[34]

$$\epsilon(k) = Ak^2 \pm [B^2k^4 + C^2(k_x^2k_y^2 + k_y^2k_z^2 + k_z^2k_x^2)]^{1/2}, \tag{11a}$$

$$\epsilon(k) = -\Delta + Ak^2, \tag{11b}$$

for the $p_{3/2}$ and $p_{1/2}$ bands, respectively. Here Δ is the spin-orbit splitting, which is[36–38] $\sim$0.3 eV; A, B, and C are the so-called inverse band mass parameters. The upper and lower signs in Eq. (11a) refer to the heavy and light holes, respectively.

The effect of an external homogeneous magnetic field and uniaxial stress on the $J=\frac{3}{2}$ band edge is obtained from the solution of the Hamiltonian

$$H = H_k + H_e, \tag{12}$$

where H_k is the $\mathbf{k}\cdot\mathbf{p}$ Luttinger Hamiltonian.[39] H_e is the strain Hamiltonian given by Kleiner and Roth[40] as

$$\begin{aligned} H_e = D_d^v(e_{xx} + e_{yy} + e_{zz}) + \tfrac{2}{3}D_u[(j_x^2 - \tfrac{1}{3}J^2)e_{xx} + \text{c.p.}] \\ + \tfrac{2}{3}D_{u'}[2\{J_xJ_y\}e_{xy} + \text{c.p.}], \end{aligned} \tag{13}$$

[28] R. N. Dexter, H. J. Zeiger, and B. Lax, Phys. Rev. **104**, 637 (1956).
[29] C. Herring, Bell System Tech. J. **34**, 237 (1955).
[30] C. Herring and E. Vogt, Phys. Rev. **101**, 944 (1956).
[31] D. K. Wilson and G. Feher, Phys. Rev. **124**, 1068 (1961); D. K. Wilson, *ibid.* **134**, A265 (1964).
[32] $e_{\alpha\beta} = \frac{1}{2}(\partial u_\alpha/\partial x_\beta + \partial u_\beta/\partial x_\alpha)$, where $\mathbf{u}$ is the displacement vector and $\mathbf{x}$ the position vector.
[33] F. Herman and J. Callaway, Phys. Rev. **89**, 518 (1953).
[34] G. Dresselhaus, A. F. Kip, and C. Kittel, Phys. Rev. **95**, 568 (1954); **98**, 368 (1955); C. Kittel, Physica **20**, 829 (1954).
[35] Γ_8^+ and Γ_7^+ are the double-group representations for the $p_{3/2}$ and $p_{1/2}$ states, respectively [see G. Dresselhaus, Ph.D. thesis, University of California, 1955 (unpublished)].
[36] A. H. Kahn, Phys. Rev. **97**, 1647 (1955), and references therein.
[37] M. V. Hobden, J. Phys. Chem. Solids **23**, 821 (1962).
[38] R. L. Aggarwal and B. Lax [Bull. Am. Phys. Soc. **11**, 828 (1966)] have determined the spin-orbit splitting $\Delta = 0.297 \pm 0.005$ eV at $T \sim 20$°K from magnetopiezoreflection experiments.
[39] J. M. Luttinger, Phys. Rev. **102**, 1030 (1956).
[40] W. H. Kleiner and L. M. Roth, Phys. Rev. Letters **2**, 334 (1959).

where D_d^v, D_u, and $D_{u'}$ are the valence-band deformation potentials. D_u and $D_{u'}$ are related to the corresponding Pikus-Bir potentials[41] b and d as $D_u=-\frac{3}{2}b$ and $D_{u'}=-\frac{1}{2}\sqrt{3}d$.[42]

It has been pointed out that for uniaxial stress along a [001] or [111] direction H_ϵ is diagonal in the representation (J,M_J), where M_J is the component of the total angular momentum J along the stress axis.[42,43] The eigenvalues of H_ϵ may be written[42,43]

$$\Delta\epsilon_v=D_d^v(e_{xx}+e_{yy}+e_{zz})\pm\{(2/9)D_u^2[(e_{xx}-e_{yy})^2+\text{c.p.}]+\tfrac{4}{3}D_{u'}^2(e_{xy}^2+\text{c.p.})\}^{1/2}. \quad (14)$$

In terms of the Pikus-Bir deformation potentials, Eq. (14) becomes

$$\Delta\epsilon_v=a(e_{xx}+e_{yy}+e_{zz})\pm\{\tfrac{1}{2}b^2[(e_{xx}-e_{yy})^2+\text{c.p.}]+d^2(e_{xy}^2+\text{c.p.})\}^{1/2}. \quad (15)$$

The last term in Eqs. (14) and (15) represents one-half the strain splitting of the $M_J=\pm\frac{3}{2}$ and $\pm\frac{1}{2}$ states, whereas the first term gives the shift in the mean energy of the split levels. It should be pointed out that Eqs. (14) and (15) are valid for a general homogeneous strain even though M_J is a good quantum number only when the uniaxial stress is along a [001] or [111] direction. If there is no strain, i.e., if $H_\epsilon=0$, the Landau-level energies are obtained from the solution of H_k. Luttinger and Kohn[26] and Luttinger[39] obtain four groups of Landau levels which are usually called the Landau ladders a^+, a^-, b^+, and b^-. The + and − refer to the light and heavy holes, respectively. In contrast to the high quantum number limit, the Landau levels in a given ladder for low quantum numbers are not equally spaced in energy.

In order to obtain the energies of the Landau levels in the presence of uniaxial stress the Hamiltonian given by Eq. (12) must be solved. This has been done by Hensel[44] for $\mathbf{H}\|\mathbf{T}\|[111]$, and by Blinowski and Grynberg[45] for $\mathbf{H}\|\mathbf{T}\|[001]$. In the high-stress limit the four Landau ladders become equally spaced with wave functions corresponding to $M_J=\frac{3}{2}$, $-\frac{3}{2}$, $\frac{1}{2}$, and $-\frac{1}{2}$, respectively. For lower stresses, the eigenvalues may be expressed in terms of a strain parameter defined as the strain splitting of the valence-band edge expressed in units of $\hbar eH/m_0c$.[44] Blinowski and Grynberg[45] have pointed out that for a [001] and [111] direction, stress does not change the structure of the wave functions which are linear combinations of the basis functions for $M_J=\frac{3}{2}$, $\frac{1}{2}$, $-\frac{1}{2}$, and $-\frac{3}{2}$ but only the amplitude of the basis functions. Also, the selection rules for electric dipole transitions to the conduction band at Γ are the same as in the unstressed case[46]: $\Delta n=0$, -2, with $\Delta M_J=0$ for $\mathbf{E}\|\mathbf{H}$ and $\Delta M_J=\pm1$ for $\mathbf{E}\perp\mathbf{H}$, where $\mathbf{E}$ is the electric vector of the incident radiation. The relative intensities of the various transitions should vary with stress.

B. Indirect Absorption Edge with Piezotransmission

The ratio of transmitted radiation to incident radiation is given by

$$T=(1-R)^2e^{-\alpha t}/1-R^2e^{-2\alpha t}, \quad (16)$$

where α is the absorption coefficient, t the sample thickness, and R the reflectivity given by

$$R=\frac{(n-1)^2+k^2}{(n+1)^2+k^2}, \quad (17)$$

where n and k are the real and imaginary parts of the complex index of refraction

$$n^*=n+ik \quad (18)$$

and

$$\alpha=4\pi k/\lambda, \quad (19)$$

where λ is the wavelength of the radiation in vacuum. If the contributions due to multiple internal reflections in the sample are neglected, Eq. (16) simplifies to

$$T\sim(1-R)^2e^{-\alpha t}. \quad (20)$$

This is a fair approximation for materials of high reflectivity like germanium for which $R\simeq0.35$ near the absorption edge.

Using Eq. (20), we may write for piezotransmission

$$\frac{\Delta T}{T}=-\frac{2R}{1-R}\frac{\Delta R}{R}-t\Delta\alpha-\alpha\Delta t. \quad (21)$$

Of the three terms contributing to $\Delta T/T$, the first is relatively small[47] and the third term merely produces a background proportional to α. Hence the spectral structure observed in $\Delta T/T$ may be attributed to the change in absorption coefficient $\Delta\alpha$ caused by the applied stress.

We will now show how the application of stress enhances the structure in α with or without the magnetic field.

Following Macfarlane and Roberts,[48] the absorption coefficient for the allowed indirect exciton in the ab-

[41] G. E. Pikus and G. L. Bir, Fiz. Tverd. Tela **1**, 1642 (1959) [English transl.: Soviet Phys.—Solid State **1**, 1502 (1959)].
[42] H. Hasegawa, Phys. Rev. **129**, 1029 (1963).
[43] J. C. Hensel and G. Feher, Phys. Rev. **129**, 1041 (1963).
[44] J. C. Hensel, Solid State Commun. **4**, 231 (1966).
[45] J. Blinowski and M. Grynberg, Phys. Status Solidi **20**, K107 (1967).
[46] L. M. Roth, B. Lax, and S. Zwerdling, Phys. Rev. **114**, 90 (1959).
[47] We have compared the reflection and transmission spectra for a (001) sample at liquid-nitrogen temperature. In the spectral region of the indirect edge, the spectral structure observed in $\Delta R/R$ was found to be an order of magnitude lower in intensity when compared with that for $\Delta T/T$ (to be published).
[48] G. G. Macfarlane and V. Roberts, Phys. Rev. **97**, 1714 (1955); **98**, 1865 (1955).

sence of an applied magnetic field may be written[49]

$$\alpha(0)=C_{\pm}[\hbar\omega-(\epsilon_g-\epsilon_{ex}\pm\epsilon_{ph})]^{1/2}, \quad (22)$$

with

$$C_{\pm}=(D/\omega)e^{\pm\hbar\omega_{ph}/kT},$$

where $\hbar\omega$ is the photon energy, ϵ_g the energy gap, ϵ_{ex} the exciton binding energy, and ϵ_{ph} the energy of the phonons which are emitted or absorbed in the process. D is a constant determined by the density of states associated with the valence and conduction bands, a product of phonon and direct-transition matrices, and a factor for multiple conduction-band minima. Therefore, the change in α due to the strain Δe is

$$\Delta\alpha(0)=-\tfrac{1}{2}C_{\pm}[\hbar\omega-(\epsilon_g-\epsilon_{ex}\pm\epsilon_{ph})]^{-1/2}d\epsilon_g/de\Delta e, \quad (23)$$

provided the stress-induced changes in ϵ_{ex} and ϵ_{ph} and $C_{\pm}$ are neglected. It is evident from Eq. (23) that the use of stress modulation technique would produce an enhancement of the structure in α, since $\Delta\alpha(0)$ has a singularity at the transition energy

$$\hbar\omega=\epsilon_g-\epsilon_{ex}\pm\epsilon_{ph}. \quad (24)$$

In the presence of a magnetic field the absorption coefficient for indirect transitions between free Landau states is given by[49]

$$\alpha(H)=2C_{\pm}(\hbar^2\omega_{c_1}\omega_{c_2})\sum_{n_1n_2}S(\hbar\omega-\hbar\omega_{n_1n_2}), \quad (25)$$

where

$$\hbar\omega_{n_1n_2}=\epsilon_g+(n_1+\tfrac{1}{2})\hbar\omega_{c_1}+(n_2+\tfrac{1}{2})\hbar\omega_{c_2}\pm\hbar\omega_{ph}+(M_2g_2-M_1g_1)\beta H.$$

Here $S(\hbar\omega-\hbar\omega_{n_1n_2})$ is a step function, ω_{c_1} and ω_{c_2} are the appropriate cyclotron frequencies for the two bands with their anisotropy taken into account, n_1 and n_2 are the respective Landau quantum numbers, g_1 and g_2 are the appropriate spin g factors, and M_1 and M_2 are the spin angular momenta. Due to the phonon transitions there are no selection rules for n_1 and n_2. However, the selection rules for the spin angular momentum are the same, with $\Delta M=0$ for $\mathbf{E}\|\mathbf{H}$ and $\Delta M=\pm1$ for $\mathbf{E}\perp\mathbf{H}$.

As in the zero-field case, the change in the absorption coefficient is given by

$$\Delta\alpha(H)\simeq 2C_{\pm}(\hbar^2\omega_{c_1}\omega_{c_2})\sum_{n_1n_2}\delta(\hbar\omega-\hbar\omega_{n_1n_2})\frac{d\epsilon_g}{de}\Delta e. \quad (26)$$

It follows from Eq. (26) that, with stress modulation, strong singularities should be observed at photon energies for which $\hbar\omega=\hbar\omega_{n_1n_2}$, in contrast to the steps observed without modulation. However, if we take into account the finite relaxation time τ for an actual crystal, the step function $S(x)\rightarrow$ arc tan$x$, where $x=(\omega-\omega_{n_1n_2})\tau$.[49] Therefore, in Eq. (26), $\delta(x)\rightarrow\tau[1+(\omega-\omega_{n_1n_2})^2\tau^2]^{-1}$. Thus the line shapes for the peaks

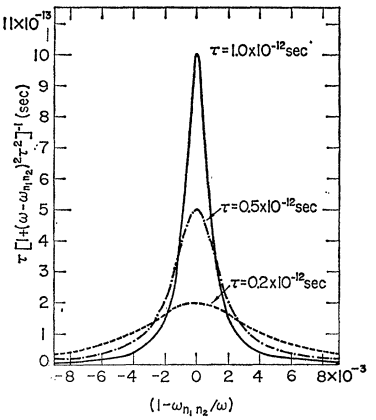

FIG. 2. Plot of $\tau[1+(\omega-\omega_{n_1n_2})^2\tau^2]^{-1}$ versus $1-\omega_{n_1n_2}/\omega$ for the relaxation time $\tau=0.2\times10^{-12}$, 0.5×10^{-12}, and 1.0×10^{-12} sec.

observed in magnetopiezotransmission should correspond to those shown in Fig. 2, where

$$\tau[1+(\omega-\omega_{n_1n_2})^2\tau^2]^{-1}$$

is plotted as a function of $1-\omega_{n_1n_2}/\omega$ for several different values of τ. As τ increases, the height of the peak increases and the half-width decreases correspondingly. Thus it should be possible to obtain an estimate for τ from the observed half-width of the peaks.

C. Nonparabolicity and Effective Masses

The most interesting feature of the present investigation for the indirect transition in germanium is the variation of the electron effective mass as a function of the energy for the electron in the L_1 conduction band. This is deduced from the observed energy spacings of the light electron peaks for the spectra shown in Figs. 5–7. We ascribe this variation to the nonparabolic character of the energy bands for increased momenta into the Brillouin zone.

The application of Brillouin-Wigner perturbation theory to nondegenerate bands in a cubic material at $k=0$ gives an energy-wave-vector relationship of the form[50]

$$\epsilon_i(k)=\epsilon_i(0)+\frac{\hbar^2k^2}{2m_0}\left(1+\frac{2}{m_0}\sum_j{}'\frac{|\pi_{ij}|^2}{\epsilon_i(k)-\epsilon_j(0)}\right), \quad (27)$$

where π_{ij} are the momentum matrix elements for coupling of the bands i and j, with $j\neq i$. It should be pointed out that the presence of the perturbed energy $\epsilon_i(k)$ in the energy denominator of Eq. (27) ensures that the nonparabolic effects are automatically included. In a similar manner, the inclusion of the nonparabolic effects in Eq. (1) for the energy of the electron in an L_1

[49] B. Lax and S. Zwerdling, in *Progress in Semiconductors*, edited by A. F. Gibson (John Wiley & Sons, Inc., New York, 1960), Vol. 5, p. 221.

[50] See, for example, G. Dresslhaus and M. S. Dresselhaus, in *Proceedings of the "Enrico Fermi" International School of Physics, Course XXXIV, 1965*, edited by J. Tauc (Academic Press Inc., New York, 1966), p. 198.

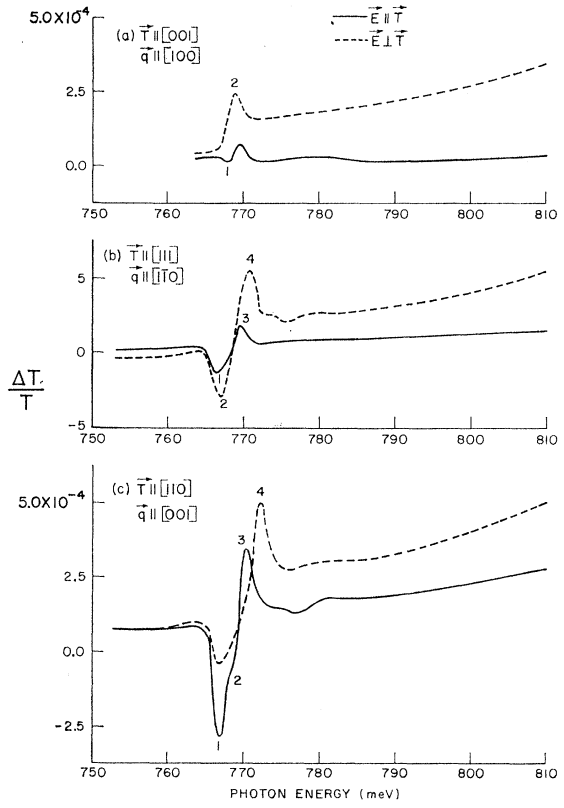

FIG. 3. Piezotransmission spectra of the indirect transition in germanium at $T\sim 20°$K for uniaxial stress **T** applied along the [001], [111], and [110] directions.

ellipsoid gives[51]

$$\mathcal{E}(k)=\frac{\hbar^2}{2m_0}(k_1^2+k_2^2)\left(1+\frac{2}{m_0}\sum_{L_3'}\frac{|\pi_{13'}|^2}{\epsilon_g(1,3')+\mathcal{E}(k)}\right)+\frac{\hbar^2k_3^2}{2m_0}\left(1+\frac{2}{m_0}\sum_{L_2'}\frac{|\pi_{12'}|^2}{\epsilon_g(1,2')+\mathcal{E}(\mathbf{k})}\right), \quad (28)$$

where $\epsilon_g(1,3')=\epsilon_{L_1}(0)-\epsilon_{L_3'}(0)$ and $\epsilon_g(1,2')=\epsilon_{L_1}(0)-\epsilon_{L_2'}(0)$; $\pi_{13'}$ and $\pi_{12'}$ denote $\pi_{L_1L_3'}$ and $\pi_{L_1L_2'}$, respectively.

Recalling the definitions of m_t and m_l, it is obvious from Eq. (28) that we now have

$$\frac{1}{m_t}=\frac{1}{m_0}\left(1+\frac{2}{m_0}\sum_{L_3'}\frac{|\pi_{13'}|^2}{\epsilon_g(1,3')+\mathcal{E}(k)}\right), \quad (29a)$$

$$\frac{1}{m_l}=\frac{1}{m_0}\left(1+\frac{2}{m_0}\sum_{L_2'}\frac{|\pi_{12'}|^2}{\epsilon_g(1,2')+\mathcal{E}(k)}\right). \quad (29b)$$

[51] In deducing Eq. (28) it is assumed that the transverse effective mass involves only the matrix elements between the bands L_1 and L_3' and the longitudinal mass is similarly determined by the matrix elements between the bands L_1 and L_2'.

TABLE II. Relative matrix elements (squared) $|M|^2$ for transitions from the $J=\frac{3}{2}$ valence band to the conduction band at Γ as the intermediate state. The initial and final states for the transitions are shown in Fig. 3. $d\epsilon_t/de$ is the change in the transition energy of a given component per unit change in the strain e along the stress axis and I represents the relative amplitude of the piezotransmission peak for the same component.

Stress direction	Component	$\lvert M\rvert^2$ E∥T	$\lvert M\rvert^2$ E⊥T	$d\epsilon_t/de$ (eV)	I E∥T	I E⊥T
[001]	1	1	$\frac{1}{4}$	1.6	−6.4	−1.6
	2	0	$\frac{3}{4}$	−5.0	0	15.0
[111]	1	1	$\frac{1}{4}$	12.8	−12.8	−3.2
	2	0	$\frac{3}{4}$	6.4	0	−4.8
	3	1	$\frac{1}{4}$	−3.6	10.8	2.7
	4	0	$\frac{3}{4}$	−10.0	0	22.5
[110]	1			6.4		
	2			−0.2		
	3			−4.6		
	4			−11.2		

Using Eqs. (29a) and (29b), Eq. (28) may be written

$$\mathcal{E}(k)=\tfrac{1}{2}\hbar^2(k_1^2+k_2^2)\times\left[\frac{1}{m_0}+\left(\frac{1}{m_t(0)}-\frac{1}{m_0}\right)\frac{\epsilon_g(1,3')}{\epsilon_g(1,3')+\mathcal{E}(k)}\right]+\frac{\hbar^2k_3^2}{2m_l}, \quad (30)$$

in the approximation that m_t is determined only by the L_3' band, which lies[11,12,14] $\sim$2.2 eV below the L_1 conduction-band minimum. In the above equation, $m_t(0)$ is the transverse mass at the bottom of the band. If the term

$$\frac{\hbar^2}{2m_0}(k_1^2+k_2^2)\left(1-\frac{\epsilon_g(1,3')}{\epsilon_g(1,3')+\mathcal{E}(k)}\right)$$

is neglected as being small, Eq. (30) simplifies to

$$\mathcal{E}(k)=\frac{\hbar^2}{2m_t(0)}(k_1^2+k_2^2)\left(1+\frac{\mathcal{E}(k)}{\epsilon_g(1,3')}\right)^{-1}+\frac{\hbar^2k_3^2}{2m_l}. \quad (31)$$

For the nonparabolic ellipsoid of Eq. (31), the energy levels in the presence of a magnetic field along the longitudinal axis of the ellipsoid are given by

$$\mathcal{E}_n\left(1+\frac{\mathcal{E}_n}{\epsilon_g(1,3')}\right)=(n+\tfrac{1}{2})\hbar\omega_c(0), \quad (32)$$

provided we neglect the spin splitting, which is small, and the terms containing k_3, since the peaks in the spectra correspond to $k_3=0$. $\omega_c(0)$ is the cyclotron frequency at the bottom of the band. Solution of the quadratic equation (32) gives

$$\mathcal{E}_n=-\tfrac{1}{2}\epsilon_g(1,3')+\tfrac{1}{2}[\epsilon_g^2(1,3')+4\epsilon_g(1,3')n\hbar\omega_c(0)]^{1/2}\times\left(1+\frac{2\hbar\omega_c(0)}{\epsilon_g(1,3')+4n\hbar\omega_c(0)}\right)^{1/2}. \quad (33)$$

Expanding the last radical on the right-hand side of the above equation, and retaining only the first two terms

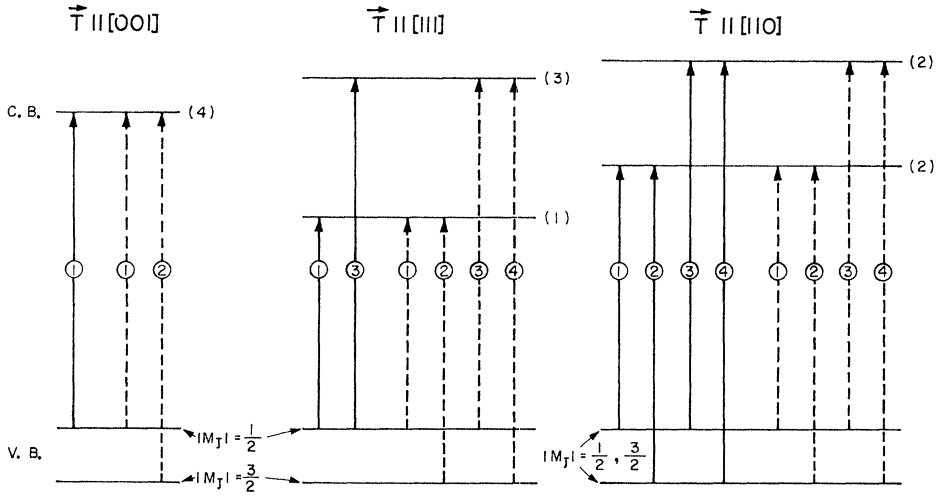

FIG. 4. Splitting of the conduction-band and valence-band edges under a [001], [111], and [110] compression (not to scale). The allowed transitions are indicated by full arrows for the electric vector $\mathbf{E}\|\mathbf{T}$ and by the dashed arrows for $\mathbf{E}\perp\mathbf{T}$. The numbers in parentheses next to the conduction-band levels denote their degeneracies.

in the expansion, we get

$$\mathcal{E}_n=-\tfrac{1}{2}\epsilon_g(1,3')+\tfrac{1}{2}[\epsilon_g^2(1,3')+4\epsilon_g(1,3')n\hbar\omega_c(0)]^{1/2}\times\left(1+\frac{\hbar\omega_c(0)}{\epsilon_g(1,3')+4n\hbar\omega_c(0)}\right). \quad (34)$$

Using Eq. (34), it can be shown that the cyclotron frequency at energies above those corresponding to the band minimum is given by

$$\omega_c=\omega_c(0)[1+2\mathcal{E}/\epsilon_g(1,3')]^{-1}. \quad (35)$$

Hence the cyclotron effective mass should increase linearly with $\mathcal{E}$ as

$$m_c=m_c(0)[1+2\mathcal{E}/\epsilon_g(1,3')]. \quad (36)$$

Using a value of 2.2 eV for $\epsilon_g(1,3')$, Eq. (36) becomes

$$m_c=m_c(0)(1+0.91\mathcal{E}), \quad (37)$$

where $\mathcal{E}$ is expressed in units of eV.

IV. EXPERIMENTAL RESULTS AND DISCUSSION

A. Piezotransmission Spectra Observed for Zero Magnetic Field

In Fig. 3 are shown the piezotransmission spectra observed with samples stressed along the [001], [111], or [110] direction. Prominent features of the spectra may be understood in terms of the transitions corresponding to the indirect exciton with the emission of a longitudinal acoustic (LA) phonon.[8] The corresponding transitions involving the absorption of an LA phonon are not observed due to the low temperatures used in the present experiments. It should be pointed out that in addition to the modulating stress, the samples may be subjected to static (dc) stress produced as a result of the unequal thermal contraction of the sample and transducer. Using the values for the expansivity of germanium[52] and of the PZT-4 transducer,[53] it turns out that the sample would be under compression if the bond between the sample and the transducer is attained at temperatures below ~160°K. In the following discussion we will assume that the samples are under compressive stress. The observed spectra are consistent with this assumption. The dc stress is along the same direction as the ac stress. This is evident from the geometry of the sample-transducer configuration as can be seen in Fig. 1.

Due to the presence of the dc stress the indirect exciton line should split into two or more components, depending upon the orientation of the applied stress. The transition energy ϵ_t for each component can be calculated from the shifts and splittings of the conduction- and valence-band edges using Eqs. (6) and (14) or (15) along with Eqs. (7), (9), and (10), provided the stress-induced changes in the phonon and the exciton binding energy are neglected. The following values have been used for the deformation potentials: $\Xi_d+\frac{1}{3}\Xi_u-a=E_1=-4$ eV,[54] $\Xi_u=16.2$ eV,[7] $b=-2.6$ eV, and $d=-4.7$ eV.[55] The results are summarized in Table II in terms of $d\epsilon_t/de$, the change in the transition energy of a given component per unit change in the strain e along the stress axis. e is related to $e_{\alpha\beta}$ as follows:

$$\begin{aligned}&\text{for } \mathbf{T}\|[001], \quad e=e_{zz},\\ &\text{for } \mathbf{T}\|[111], \quad e=\tfrac{1}{3}[(e_{xx}+e_{yy}+e_{zz})+2(e_{xy}+e_{yz}+e_{zx})],\\ &\text{for } \mathbf{T}\|[110], \quad e=\tfrac{1}{2}[(e_{xx}+e_{yy})+2e_{xy}].\end{aligned} \quad (38)$$

The expected number of components along with their initial and final states are shown in Fig. 4. The relative

[52] D. F. Gibbons, Phys. Rev. 112, 136 (1958).

[53] The expansion coefficient α_1 of poled PZT-4 (in the plane normal to the direction of polarization) is estimated to be ~2 $\times10^{-6}$/°C in the temperature range 300–4°K according to D. Berlincourt, Electronic Research Division, Clevite Corporation, Bedford, Ohio.

[54] W. Paul, J. Phys. Chem. Solids 8, 196 (1959).

[55] A. P. Smith, M. Cardona, and F. H. Pollak, Bull. Am. Phys. Soc. 12, 101 (1967).

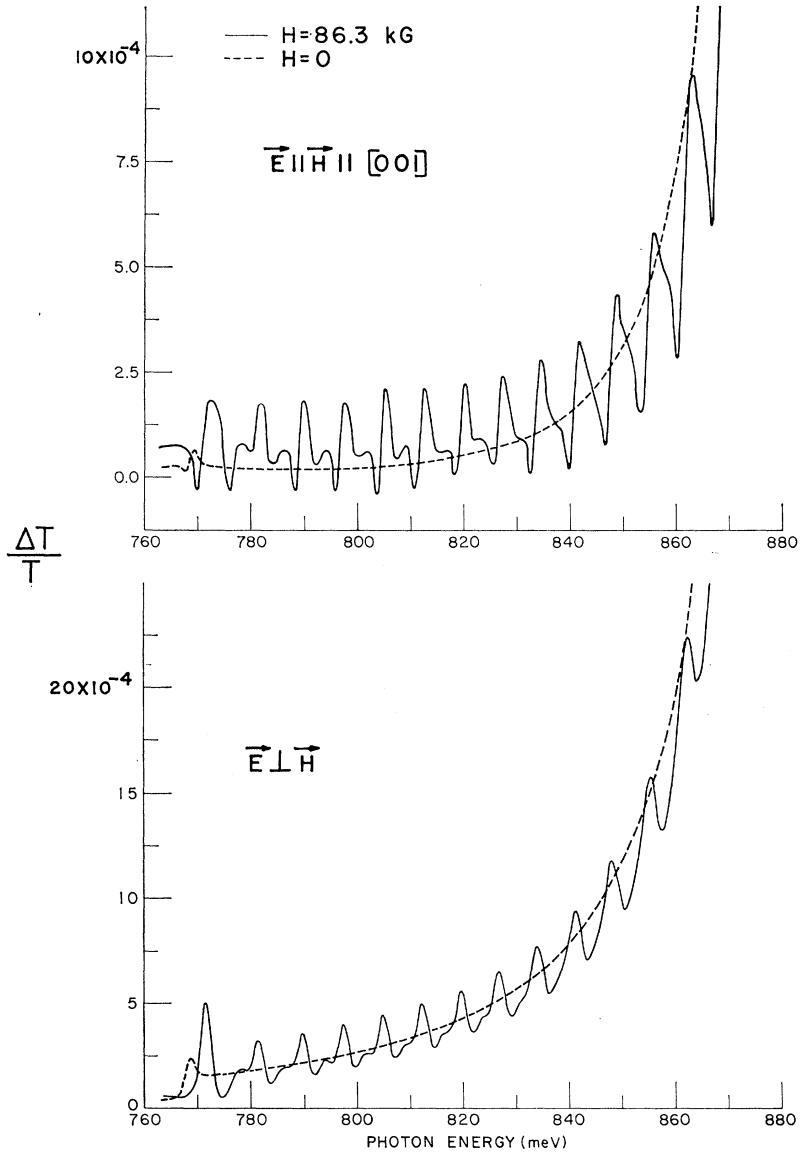

FIG. 5. Magnetopiezotransmission spectra of the indirect transition in germanium at $T\sim 20°K$ for $\mathbf{H}\|\mathbf{T}\|[001]$ with $\mathbf{q}\|[100]$, where $\mathbf{q}$ is the direction of light propagation.

intensities of these components may be estimated in the following manner. If the transitions take place via the $k=0$ conduction-band minimum as the intermediate state, it is easy to calculate the relative matrix elements for the various components. This was first done by Adler and Erlbach,[56] using group-theoretical techniques for stress parallel to [001] and [111] directions. Their results are summarized in Table II. In addition to the matrix elements, the relative intensities depend upon the density of states of the initial and final levels, and upon $d\epsilon_t/de$ when the stress modulation technique is used. It is the sign of $d\epsilon_t/de$ which determines whether a given transition would be observed as a positive or negative peak in piezotransmission. Neglecting the first and third terms on the right-hand side of Eq. (21), the relative amplitude I of a given peak due to resonant absorption may be written

$$I=N_c|M|^2\frac{d\epsilon_t}{de}, \tag{39}$$

where N_c denotes the number of the conduction-band ellipsoids which may participate in the given transition, and $|M|^2$ the squares of the relative matrix elements for transitions to the lowest conduction band at $k=0$ as the intermediate state. In writing Eq. (39), it is assumed that the phonon matrices are the same for all the components. Also, any correction due to the density-of-states weighting factor is not included. A comparison of the observed spectra with those expected from the above analysis is given below.

[56] E. Adler and E. Erlbach, Phys. Rev. Letters **16**, 87 (1966); **16**, 927 (1966).

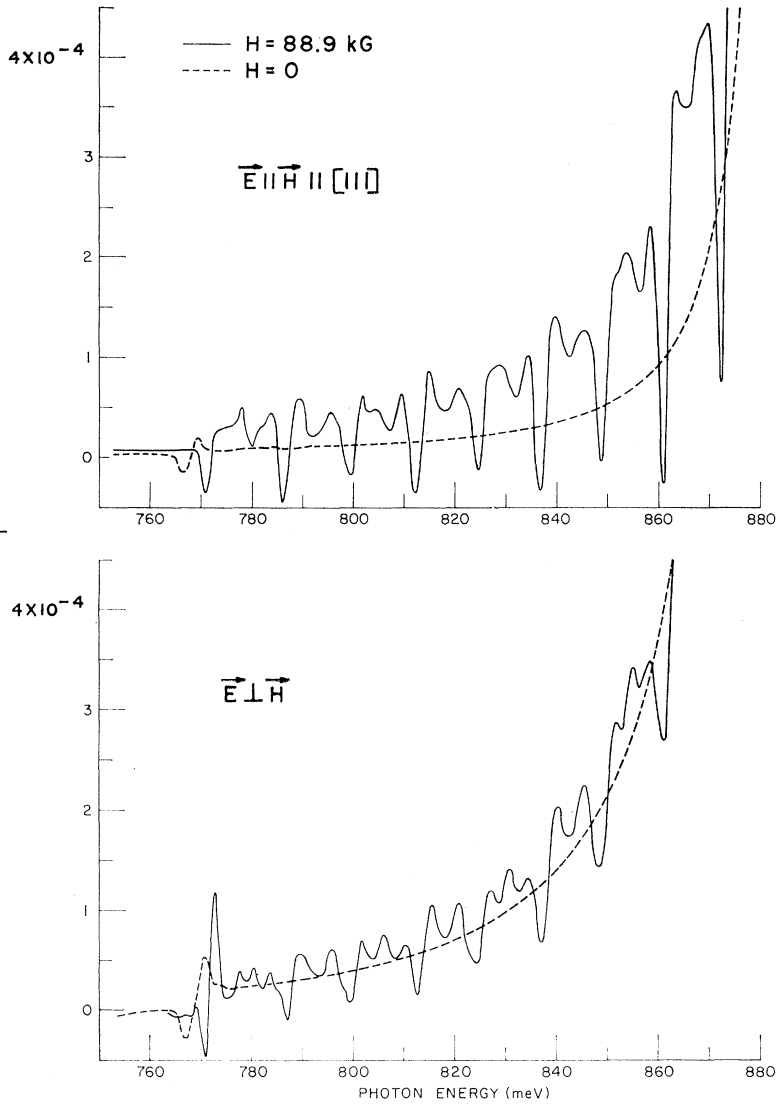

FIG. 6. Magnetopiezotransmission spectra of the indirect transition in germanium at $T\sim 20°K$ for $\mathbf{H}\|\mathbf{T}\|[111]$ with $\mathbf{q}\|[1\bar{1}0]$.

1. [001] Stress

According to the results summarized in Table II for the intensities of the stress-induced components, I should be equal to 15.0 for the high-energy components and -1.6 for the low-energy component with $\mathbf{E}\perp\mathbf{T}$. Since the low-energy component is expected to be very weak in comparison to the high-energy component, only the latter may be observed. This is actually the case experimentally as can be seen from Fig. 3(a). For $\mathbf{E}\|\mathbf{T}$, I should be zero for the high-energy component and -6.4 for the low-energy component. Thus we should observe only the low-energy component in this case. Experimental results shown in Fig. 3(a) do not agree with the above prediction since not only is the low-energy component much weaker than that expected, but a peak on the high-energy side is also observed. The high-energy peak, however, does not occur at the same position as the high-energy peak in the case of the perpendicular polarization. The former is ~ 1 meV higher in energy relative to the latter, which indicates that they do not arise from a common transition.

The observed splitting of ~ 1.3 meV between the high-energy component for $\mathbf{E}\perp\mathbf{T}$ and the low-energy component observed with $\mathbf{E}\|\mathbf{T}$ should be equal to the splitting of the $J=\frac{3}{2}$ valence-band levels $|M_J|=\frac{3}{2}$ and $\frac{1}{2}$ for a [001] stress. Using the values of $d\epsilon_t/de$ for the high- and low-energy components, we deduce that the splitting of 1.3 meV corresponds to a static strain $e\simeq 2.0\times 10^{-4}$ which would be produced by the stress $T\simeq 2.0\times 10^{8}$ dyn/cm^2 along the [001] direction.[57] It should be pointed out that the above value of dc strain

[57] The dc strain introduced in the sample is not reproducible. Variations of the order of 50% may be obtained between runs repeated on the same sample under similar conditions.

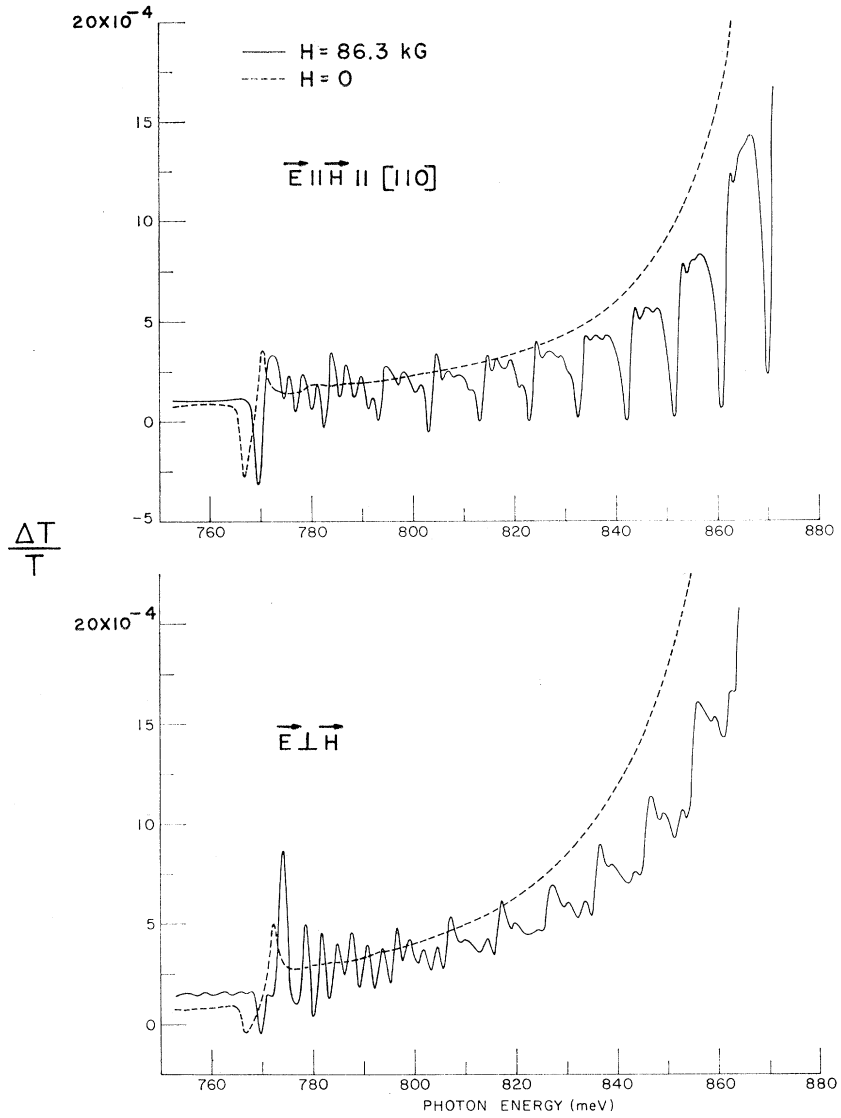

FIG. 7. Magnetopiezotransmission spectra of the indirect transition in germanium at $T\sim 20°K$ for $\mathbf{H}\|\mathbf{T}\|[110]$ with $\mathbf{q}\|[001]$.

in the sample is an order of magnitude larger than the rms value of $\sim 2.5\times 10^{-5}$ for the ac strain used in the present experiments.

2. [111] Stress

A total of four components are expected in this case as shown in Fig. 4. For $\mathbf{E}\perp\mathbf{T}$, I should be equal to -3.2, -4.8, 2.7, and 22.5 for the components labeled as 1, 2, 3, and 4 in Fig. 4. In the case of $\mathbf{E}\|\mathbf{T}$, I should be -12.8, 0, 10.8, and 0, respectively, for the same components. The observed spectra shown in Fig. 3(b) seem to indicate the presence of the four components as expected, but their relative intensities are not in good agreement with the predicted values. Weak structure observed on the high-energy side of the component 4 may be due to phonon modes other than LA mode.

The energy separation between the various components may be used to estimate the amount of static stress on the sample. The observed splitting of ~ 4.1 meV between the components 1 and 4 corresponds to a strain $e\simeq 1.8\times 10^{-4}$ or stress $T\simeq 2.8\times 10^{8}$ dyn/cm^2 along the [111] axis.[57]

3. [110] Stress

For this orientation of stress, M_J is not a good quantum number for the stress-split $J=\frac{3}{2}$ valence-band edge as mentioned earlier. Thus there are no selection rules for the matrix elements for transitions to the intermediate state assumed to be the conduction band at $k=0$, and a maximum of four components could be expected for either polarization of $\mathbf{E}$ relative to $\mathbf{T}$. The observed spectra shown in Fig. 3(c) indicate that the

components 1 and 3 are clearly resolved for $\mathbf{E}\|\mathbf{T}$, whereas the components 1 and 4 are observed with $\mathbf{E}\perp\mathbf{T}$. Other components are not resolved as well. As in the case of the [111] stress, weak structure on the high-energy side of the component 4 is due to other phonons.

The energy separation between the components 1 and 4 is ~ 5.3 meV, which corresponds to the static strain $e \simeq 3.0\times10^{-4}$ or the stress $T \simeq 4.1\times10^{8}$ dyn/cm^2 along the [110] direction.[57]

B. Magnetopiezotransmission Spectra

In Figs. 5–7 are shown the piezotransmission spectra recorded with light polarized either parallel or perpendicular to the magnetic field applied along a [001], [111], or [110] direction. In each case, uniaxial stress is parallel to the magnetic field. For all the three crystal orientations relative to the magnetic field, the spectra exhibit one or more series of sharp peaks which are resolved even at photon energies close to the direct edge. The peaks have a half-width of ~ 2 meV, which corresponds to a value of 2.5×10^{-3} for $\Delta\omega/\omega$. From the curves shown in Fig. 2, we estimate $\tau \simeq 0.7\times10^{-12}$ sec for the observed value of $\Delta\omega/\omega$. A detailed account of the magnetopiezotransmission spectra for each orientation of the magnetic field is given below.

1. H and T Parallel to [001]

For either polarization of the incident radiation, there are two series of peaks with nearly equal spacing between the consecutive peaks. The corresponding peaks of the two series are, however, displaced from each other by ~ 2 meV. Furthermore, the energy separation of the peaks in a given series corresponds to the cyclotron frequency ω_c of the conduction electrons. Thus each series of peaks may be interpreted as arising from either a single Landau level or a group of Landau levels in the valence band whose energies may lie in an interval of approximately 1 meV, which is the resolution of the spectrometer for the conditions under which the spectra shown in Figs. 5–7 were recorded. The two series of peaks may be due to transitions from the lowest Landau levels which correspond to the two states for the stress-split valence-band edge in the absence of the magnetic field. But it is not obvious why transitions from higher valence-band Landau levels are not observed. It may be due to the fact that the intermediate transition which involves the direct exciton bound to the lowest Landau levels is considerably stronger compared with direct transitions between higher Landau levels. Thus the indirect transitions from the higher valence-band levels should be comparatively weak and may not be observed.

2. H and T Parallel to [111]

In this case, one series of strong negative peaks with large energy spacing and another series of weak peaks

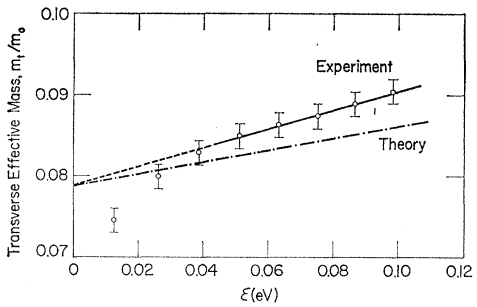

FIG. 8. Plot of the transverse effective mass m_t for the L_1 conduction band in germanium at $T\sim20$°K for $\mathbf{H}\|[111]$ as a function of $\mathcal{E}$, where $\mathcal{E}$ is the energy measured from the bottom of the band. The circles denote the experimental points for $H=88.9$ kG with $\mathbf{E}\|\mathbf{H}$. The experimental curve is a least-squares fit of the data points to a straight line. The dashed part of this line is to indicate the data points not included for the fit. The theoretical curve shows the effective-mass variation as obtained from Eq. (37), which was deduced from the use of the $\langle\mathbf{k}\cdot\mathbf{p}\rangle$ perturbation theory.

with smaller energy spacing are observed for both $\mathbf{E}\|\mathbf{H}$ and $\mathbf{E}\perp\mathbf{H}$. The sign of peaks in the weak series is ambiguous. A comparison of the observed spacings with those expected for the conduction electron shows that the peaks with large spacing arise from transitions to the Landau levels corresponding to the light electron mass m_{le}. Similarly, the peaks with small spacing are ascribed to the heavy electron mass m_{he}. As in the case of $\mathbf{H}\|[001]$, each series of peaks appears to be due to transitions from the lowest Landau levels of the valence band.

3. H and T Parallel to [110]

As in the previous case, two series of peaks with different energy spacing are observed. An interesting feature of this orientation of the magnetic field is the strong dependence of the intensity of the peaks in the two series on the direction of polarization of the radiation relative to the magnetic field. For example, peaks with small spacing are much more prominent in the spectrum for $\mathbf{E}\perp\mathbf{H}$ than in that for $\mathbf{E}\|\mathbf{H}$, as can be seen from Fig. 7. On the other hand, the negative peaks with large spacing have larger amplitude for $\mathbf{E}\|\mathbf{H}$ compared with the spectrum for $\mathbf{E}\perp\mathbf{H}$. These features are consistent with those corresponding to the zero-field case in that the positive peak is stronger for $\mathbf{E}\perp\mathbf{T}$ whereas the negative peak is stronger for $\mathbf{E}\|\mathbf{T}$. As in the case for $\mathbf{H}\|[111]$, the peaks with the large spacing are interpreted as arising from transitions to the Landau levels corresponding to m_{le}. Similarly, the peaks with the small spacing correspond to m_{he}.

C. Conduction-Band Effective Masses

The energy spacings between the successive peaks of the light-mass series for the spectra shown in Figs. 5–8 can be used for deducing the light electron mass as a function of the electron energy above that at the bottom of the band.

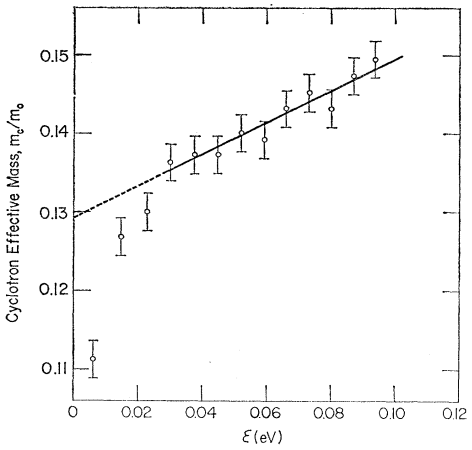

FIG. 9. Plot of the cyclotron effective mass m_c for the L_1 conduction band in germanium at $T\sim 20°K$ for $\mathbf{H}\|[001]$ as a function of $\mathcal{E}$. The circles represent the experimental points for $\mathbf{E}\perp\mathbf{H}$ with $H=86.3$ kG. The curve is a least-squares fit of the data to a straight line. The dashed part of the line is to indicate the data points not used for the fit.

The variation of the transverse effective mass m_t, which is the same as m_{le} for $\mathbf{H}\|[111]$, is shown in Fig. 8 as a function of $\mathcal{E}$. Since the heavy electron mass $m_{he}\simeq 2.5m_t$ for this orientation of the magnetic field, it implies that every alternate peak due to m_{le} may overlap another peak due to m_{he}, resulting in a distortion of the observed peak. This appears to be the case experimentally. As can be seen from the spectra shown in Fig. 6, each alternate peak corresponding to the large spacing is noticeably broad for $\mathbf{E}\perp\mathbf{H}$ and the corresponding peaks for $\mathbf{E}\|\mathbf{H}$ alternate in intensity. In order to avoid any error introduced by the above overlap, we have deduced the values of m_t shown in Fig. 8 from the energy spacing between alternate peaks instead of that between the consecutive peaks. The experimental curve is a least-squares fit of the data to a straight line. The dashed part of the line is to indicate the range of $\mathcal{E}$ which is not used for the fit. Figure 8 shows that the increase in mass is linear only for large values of $\mathcal{E}$, and the observed increase is larger than expected from Eq. (37) since the least-squares fit gives

$$m_t=m_t(0)(1+1.5\mathcal{E}).$$

The apparent departure from linearity for small values of $\mathcal{E}$ can be understood if the interband magneto-optical transitions correspond to the creation of exciton states in a magnetic field. If the Coulomb binding energy decreases with increasing n, the effective mass deduced from the observed spectra should approach the true effective mass for large n. Since the exact variation of the exciton binding energy is not known, the mass at the bottom of the band has been determined by extrapolation of the line obtained for large $\mathcal{E}$. In this manner, we obtain $m_t(0)=(0.079\pm 0.001)m_0$. This is to be compared with the value of $0.082m_0$ as obtained from the cyclotron resonance experiments.[28,34] The above discrepancy may partly be due to the neglect of Coulomb binding energy, which may be appreciable even for large n.

TABLE III. Effective masses for the L_1 conduction band in germanium.

Effective mass	Cyclotron resonance (4°K)	Magneto-absorption[a] (1.7°K)	Magnetopiezo-transmission (20°K)
$m_t(0)/m_0$	0.0819 ± 0.0003[b] $0.082\ \pm 0.001$[c]	0.079	0.079 ± 0.001
m_l/m_0	$1.64\ \pm 0.03$[b] $1.58\ \pm 0.04$[c]	1.74	$1.54\ \pm 0.06$

[a] Reference 6.
[b] Reference 28.
[c] Reference 34.

In Fig. 9 is shown the variation of the cyclotron effective mass as a function of $\mathcal{E}$ for $\mathbf{H}\|[001]$ as obtained from the spectrum for $\mathbf{E}\perp\mathbf{H}$. As in the case of $\mathbf{H}\|[111]$, m_c is deduced from the energy spacing between the alternate peaks but only to reduce scatter in the data. A least-squares fit for the data gives

$$m_c=m_c(0)(1+1.6\mathcal{E}),$$

with $m_c(0)=(0.128\pm 0.002)m_0$. Assuming the ratio $m_l/m_t\simeq 20$,[28] Eq. (4) gives $m_t(0)=(0.078\pm 0.002)m_0$ for the above value of $m_c(0)$. This value of $m_t(0)$ is in good agreement with that obtained for $\mathbf{H}\|[111]$.

In Fig. 10 is shown a plot of m_{le} as a function of $\mathcal{E}$ for $\mathbf{H}\|[110]$ with $\mathbf{E}\|\mathbf{H}$. m_{le} is deduced from the energy spacing between the alternate peaks instead of that bebetween the consecutive peaks. As in the previous cases, a linear fit to the data gives

$$m_{le}=m_{le}(0)(1+1.5\mathcal{E}),$$

with $m_{le}(0)=(0.079\pm 0.001)m_0$, which is in good agreement with the value obtained for $\mathbf{H}\|[111]$.

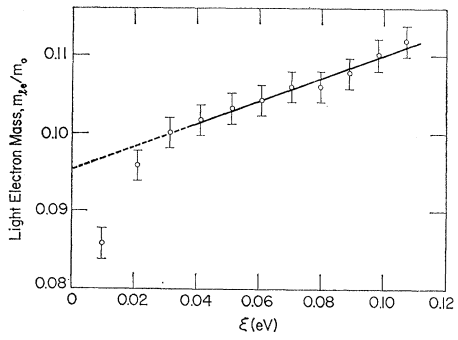

FIG. 10. Plot of the light electron mass m_{le} corresponding to $\mathbf{H}\|[110]$ for the L_1 conduction band in germanium at $T\sim 20°K$ as a function of $\mathcal{E}$. The circles represent the experimental points for $\mathbf{E}\|\mathbf{H}$ with $H=86.3$ kG. The curve is a least-squares fit of the data points to a straight line. The dashed part of the line is to indicate the data points not used for the fit.

A similar analysis for the variation of the heavy electron mass with $\mathcal{E}$ has not been attempted, since the corresponding peaks in the spectra are not resolved over a large spectral range. However, an average value of m_{he} may be used for a determination of m_l. Considering the case of $\mathbf{H}\|[110]$ with $\mathbf{E}\perp\mathbf{H}$, we get an average value of $m_{he}=(0.352\pm0.006)m_0$ on the basis of the first 10 peaks, excluding that due to the lowest ($n=0$) exciton. Using an average value of $0.081m_0$ for m_t as expected from the variation shown in Fig. 10, we find $m_l=(1.54\pm0.06)m_0$.

Table III gives a summary of the conduction-band-edge effective masses obtained from the present work along with the results of cyclotron resonance[28,34] and magnetoabsorption experiments.[6]

ACKNOWLEDGMENTS

We wish to express our gratitude to Dr. G. Dresselhaus for many stimulating discussions, to Dr. J. Halpern and K. J. Button for useful comments, and to U. Smith for a critical reading of the manuscript. We would like to thank L. V. Sousa for technical assistance with the experiments, R. Arndt for the assembly of the digital data recording system, D. R. Nelson for the computer program for data reduction, and W. Tice for x-ray orientation of the samples.

PHYSICAL REVIEW VOLUME 180, NUMBER 3 15 APRIL 1969

Magnetic Freeze-Out of Electrons in Extrinsic Semiconductors

M. I. DYAKONOV, A. L. EFROS, AND D. L. MITCHELL*
A. F. Ioffe Physical Technical Institute, Leningrad, U.S.S.R.
(Received 16 October 1968)

The density of states was derived and the statistics of conduction electrons were studied for the case of a strongly doped compensated semiconductor in an external magnetic field. The tail of the density of states and the spread in the energy distribution of impurity levels were investigated, and the temperature and magnetic field dependences of the concentration of electrons not localized in impurities were calculated. It is shown that, because of the tail of the density of states, this concentration approaches a finite limit when $T\to0$. The freeze-out of carriers begins when the magnetic field attains such a value that the binding energy becomes larger than the rms potential energy of an electron in the field of the impurities. For sufficiently large magnetic fields, the Fermi level will drop into the tail, although the electrons may remain degenerate. This last conclusion will also be true for uncompensated semiconductors.

I. INTRODUCTION

IN semiconductors with shallow donor (acceptor) levels the impurity band emerges with the conduction band at comparatively low impurity concentrations. It has been pointed out previously[1–3] that the impurity band will split off in sufficiently strong magnetic fields. This is because of the disappearance of the overlap of electronic wave functions situated on neighboring impurity sites due to their constriction to a cigar-shaped region under the influence of the magnetic field. The radius of this region is of the order of the magnetic length $\lambda=(\hbar c/eH)^{1/2}$ which may become much smaller than the Bohr radius a. Thus, localized states with a binding energy which increases with magnetic field will appear[1,4,5] when the volume of the bound state ($\pi\lambda^2a$) becomes less than the average volume of an impurity (N^{-1}), i.e., $N\pi\lambda^2a<1$.

This behavior becomes evident in the freeze-out effect, i.e., the electron concentration begins to depend on the temperature and magnetic field. This effect was studied in InSb by Sladek[3] and later by Beckman *et al.*[6] and by Neuringer.[7] In earlier works,[2,3] a theory for this effect was proposed which did not take into account the shifts in the impurity levels due to the random impurity potential. This is valid only for very lightly doped semiconductors when the rms potential of impurities is small compared to the binding energy of the electrons $\mathcal{E}_b$ and the thermal energy T (in units of energy).

In the present paper, we calculate the density of states of a strongly doped semiconductor in a magnetic field and construct the theory for freezing out. The tail of the density of states of electrons in a magnetic field

* Visiting scientist under the exchange program between the National Academy of Sciences U.S.A. and the Academy of Sciences U.S.S.R. On leave from the Naval Research Laboratory, Washington, D. C.

[1] Y. Yafet, R. W. Keyes, and E. N. Adams, J. Phys. Chem. Solids **1**, 137 (1956).

[2] R. W. Keyes and R. J. Sladek, J. Phys. Chem. Solids **1**, 143 (1956).

[3] R. J. Sladek, J. Phys. Chem. Solids **5**, 157 (1958).

[4] H. Hasegawa and R. E. Howard, J. Phys. Chem. Solids **21**, 179 (1961).

[5] R. J. Elliot and R. Loudon, J. Phys. Chem. Solids **15**, 196 (1960); R. F. Wallis and H. J. Bowlden, *ibid.* **7**, 78 (1958).

[6] O. Beckman, E. Hanamura, and L. J. Neuringer, Phys. Rev. Letters **18**, 773 (1967).

[7] L. J. Neuringer, in *Proceedings of the International Conference on the Physics of Semiconductors, Moscow, 1968* (Publishing House Nauka, Leningrad, 1968), p. 715.